

Geophysical Research Letters®



RESEARCH LETTER

10.1029/2025GL117647

Key Points:

- Data-assimilated convection improves agreement of modeled and EISCAT-derived Joule heating rates by up to 54% compared to empirical models
- The recently released Thermosphere Ionosphere Electrodynamics General Circulation Model version 3.0 shows Joule heating rates increased by 20% due to higher grid resolution
- Internal model time step size does not affect the model Joule heating rates

Correspondence to:

F. Günzkofer,
florian.guenzkofer@dlr.de

Citation:

Günzkofer, F., Liu, H., Liu, H., Stober, G., Lu, G., Wu, H., et al. (2025). High-latitude Joule heating in TIE-GCM 3.0: Evaluation of different plasma convection forcing models. *Geophysical Research Letters*, 52, e2025GL117647. <https://doi.org/10.1029/2025GL117647>

Received 17 JUN 2025
Accepted 19 AUG 2025









Author Contributions:

Conceptualization: Florian Günzkofer, Hanli Liu, Huixin Liu, Gunter Stober
Data curation: Gang Lu, Haonan Wu, Nicholas Bartel, Frank Heymann
Formal analysis: Florian Günzkofer
Funding acquisition: Hanli Liu, Huixin Liu, Claudia Borries
Investigation: Florian Günzkofer
Methodology: Florian Günzkofer, Hanli Liu, Huixin Liu, Gunter Stober
Project administration: Hanli Liu, Huixin Liu
Resources: Hanli Liu, Gang Lu, Haonan Wu, Nicholas Bartel, Frank Heymann
Software: Florian Günzkofer
Supervision: Hanli Liu, Huixin Liu, Gunter Stober, Claudia Borries
Validation: Florian Günzkofer, Gunter Stober, Gang Lu, Haonan Wu
Visualization: Florian Günzkofer
Writing – original draft: Florian Günzkofer, Gunter Stober

© 2025. The Author(s).

This is an open access article under the terms of the [Creative Commons Attribution License](#), which permits use, distribution and reproduction in any medium, provided the original work is properly cited.

High-Latitude Joule Heating in TIE-GCM 3.0: Evaluation of Different Plasma Convection Forcing Models

Florian Günzkofer¹ , Hanli Liu² , Huixin Liu³ , Gunter Stober^{4,5}, Gang Lu² , Haonan Wu² , Nicholas Bartel⁶ , Frank Heymann¹ , and Claudia Borries¹ 

¹Institute for Solar-Terrestrial Physics, German Aerospace Center (DLR), Neustrelitz, Germany, ²High Altitude Observatory, National Center for Atmospheric Research, Boulder, CO, USA, ³Department of Earth and Planetary Science, Kyushu University, Fukuoka, Japan, ⁴Institute of Applied Physics, Microwave Physics, University of Bern, Bern, Switzerland, ⁵Oeschger Center for Climate Change Research, Microwave Physics, University of Bern, Bern, Switzerland, ⁶University of Colorado Boulder, Boulder, CO, USA

Abstract We systematically evaluate the high-latitude Joule heating of the recently released version 3.0 Thermosphere Ionosphere Electrodynamics General Circulation Model (TIE-GCM) by comparison to EISCAT incoherent scatter radar measurements. The model performance is examined using normalized root mean square deviations derived from test runs driven by different convection patterns from empirical and data-assimilated models. The following features are revealed: (a) Data-assimilated geomagnetic forcing improves the agreement between modeled and EISCAT-derived Joule heating rates by 8%, 28%, and 54% for low, moderate, and high geomagnetic activity. (b) Increasing model grid resolution from 2.5° to 1.25° leads to ~20% higher Joule heating rates. (c) AMIE-driven runs better reproduce the magnitude of the Joule heating rates, AMGeO-driven runs the vertical profile. (d) Internal model time step resolution has no effect on the Joule heating rates.

Plain Language Summary In the polar regions of the ionosphere, there is an electric potential difference between the dawn side (“positive pole”) and the dusk side (“negative pole”). Electric currents along the associated electric fields heat the upper atmosphere, similar to a power wire being heated. Models of the upper atmosphere can estimate this Joule heating, though their accuracy varies strongly. We evaluate the Joule heating rates of the Thermosphere Ionosphere Electrodynamics General Circulation Model for multiple model settings to assess which settings give the presumably most accurate Joule heating rates under which conditions.

1. Introduction

The high-latitude plasma convection gives rise to Pedersen and Hall currents that peak in the E region of the ionosphere. These currents cause Joule heating of the thermosphere-ionosphere system and geomagnetic disturbances. Previous studies investigated the global pattern of height-integrated Joule heating rates derived from satellite measurements (e.g., Kauristie et al., 2024; Palmroth et al., 2005; Rich et al., 1991) and the vertical Joule heating rate profiles derived from incoherent scatter radar (ISR) measurements (e.g., Baloukdis et al., 2023; Günzkofer et al., 2024; Kavanagh et al., 2022; Thayer, 2000). Thermosphere-ionosphere models are known to have difficulties with representing high-latitude Joule heating rates (Baloukdis et al., 2023; Codrescu et al., 1995; Emery et al., 1999; Günzkofer et al., 2024). Hence, systematic model evaluations are required to assess potential shortcomings and derive proper mitigation by parameterizing or a more physically consistent description of the Joule heating.

Günzkofer et al. (2024) suggested adjusting the empirical Joule heating scaling factor of the Thermosphere Ionosphere Electrodynamics General Circulation Model (TIE-GCM) (Codrescu et al., 1995; Richmond et al., 1992) based on 2,000 hr of measurements with the EISCAT ultra-high frequency ISR. However, Codrescu et al. (2000) showed that the short-scale variability of the electric field changes with geomagnetic latitude and local magnetic time. A globally constant scaling factor is therefore limited in its applicability, and adjusting it based on local measurements might not lead to improvements.

This study provides a general overview of how well the model reproduces locally measured Joule heating rates for different model settings and geomagnetic forcing methods. A special focus is on the recently (May 2024) released TIE-GCM version 3.0 (Wu et al., 2025). This version includes changes to the physics, as well as the option to perform model runs with an increased horizontal resolution of 1.25°. We will systematically assess the impact of

Writing – review & editing: Hanli Liu, Huixin Liu, Gunter Stober, Gang Lu, Haonan Wu, Nicholas Bartel, Frank Heymann, Claudia Borries

the model version and grid resolution on the Joule heating rates. While previous studies mostly investigated a single plasma convection model, we aim to give a systematic overview of four convection models and their impact on the Joule heating rates.

The applied methodology is equivalent to the analysis presented in Günzkofer et al. (2024). Both EISCAT plasma parameters and model outputs are binned in 5 km steps from 95–125 km altitudes and 10 km steps from 135–185 km. The Joule heating rate profile is calculated as

$$q_J = \left(\frac{\nu_{en}}{\nu_{en}^2 + \omega_e^2} + \frac{m_e}{m_i} \frac{\nu_{in}}{\nu_{in}^2 + \omega_i^2} \right) \frac{N_e e^2}{m_e} \cdot (\vec{E} + \vec{u} \times \vec{B})^2. \quad (1)$$

In Equation 1, only the electron density N_e and the electric field \vec{E} are obtained from ISR observations. The other parameters—electron/ion-neutral collision frequency $\nu_{en/in}$, electron/ion gyrofrequency $\omega_{e/i}$, mean ion mass m_i , and neutral wind \vec{u} —are taken from the model output. Hence, the “measurement/EISCAT” Joule heating profile has to be calculated separately for each investigated model run (Günzkofer et al., 2024). The electron mass m_e and charge e are fundamental constants, and the magnetic field \vec{B} is obtained from the IGRF (Alken et al., 2021). To assess how well the model profile q_J^m resembles the “measurement/EISCAT” Joule heating profile q_J^E , we will apply the *normalized root mean square deviation*

$$\epsilon_N = \frac{\sqrt{\text{mean}((q_J^E - q_J^m)^2)}}{\max(q_J^E)}. \quad (2)$$

Introducing the normalization allows comparison of different geomagnetic activity levels without suffering from the different energy scales. As in Günzkofer et al. (2024), we will determine an “adjusted scaling factor” f obtained from a non-linear least-squares fit of $q_J^E - f \cdot q_J^m = 0$. This will allow distinguishing model runs that reproduce the shape of the Joule heating profile well, as for these runs ϵ_N will be significantly decreased when applying the adjusted scaling factor.

Section 2 presents a summary of the EISCAT Ultra High Frequency (UHF) radar, the TIE-GCM, and the four convection models applied for high-latitude geomagnetic forcing. In Section 3, we will present the obtained variations of Joule heating rates with model version, grid resolution, and convection model. Section 4 will conclude the paper, discuss the presented results, and give an outlook on future work.

2. Measurements and Models

2.1. EISCAT UHF Radar

We analyze measurements collected with the EISCAT Ultra High Frequency (UHF, 930 MHz) ISR at Tromsø, Norway (69.6°N, 19.2°E) (Folkestad et al., 1983). The radar dish has a diameter of 32 m, resulting in a beam width of about 0.7° corresponding to an antenna directive gain of approximately 48.1 dBi. Since the EISCAT radars are operated campaign-based, the database contains only a small number of continuous measurements to study the Joule heating. In this study, we leverage two EISCAT UHF campaigns from 9 to 28 September 2005 (456 hr, Nozawa et al., 2010) and 14 to 25 September 2009 (240 hr). Larger databases are available (e.g., Baloukidis et al., 2023; Günzkofer et al., 2024) but we restricted the analysis to these two campaigns to limit the required modeling resources (see Section 2.2).

The radar was operated in the *Common Programme (CP) 2*, also often referred to as *beam-swing* mode (Kavanagh et al., 2022). Line-of-sight ion velocity measurements from the four radar pointing directions are converted to 3D ion velocity vectors applying the stochastic inversion technique introduced by Nygrén et al. (2011). The electric field is calculated from the F region ion velocity and propagated into the E region, that is, it increases slightly $\propto 1/B$. The E region neutral winds are explicitly not inferred with the method by Nygrén et al. (2011) since this would require longer integration times.

Table 1
List of the 19 Investigated Thermosphere Ionosphere Electrodynamics General Circulation Model Runs

Run#	Dates	Convection	Version	Resolution	Internal time step (s)
#1	9–28 September 2005	Heelis	3.0	$2.5^{\circ} \times 2.5^{\circ}$	10–30
#2	9–28 September 2005	Heelis	3.0	$1.25^{\circ} \times 1.25^{\circ}$	5–30
#3	9–28 September 2005	Heelis	2.0	$2.5^{\circ} \times 2.5^{\circ}$	10–30
#4	9–28 September 2005	Weimer	3.0	$2.5^{\circ} \times 2.5^{\circ}$	10–30
#5	9–28 September 2005	Weimer	3.0	$1.25^{\circ} \times 1.25^{\circ}$	5–30
#6	9–28 September 2005	Weimer	2.0	$2.5^{\circ} \times 2.5^{\circ}$	10–30
#7	9–16 September 2005	AMIE	3.0	$2.5^{\circ} \times 2.5^{\circ}$	10–30
#8	9–16 September 2005	AMIE	3.0	$1.25^{\circ} \times 1.25^{\circ}$	5–30
#9	9–16 September 2005	AMIE	2.0	$2.5^{\circ} \times 2.5^{\circ}$	10–30
#10	9–28 September 2005	AMGeO	3.0	$2.5^{\circ} \times 2.5^{\circ}$	10–30
#11	9–28 September 2005	AMGeO	3.0	$1.25^{\circ} \times 1.25^{\circ}$	10–30
#12	14–25 September 2009	Heelis	3.0	$2.5^{\circ} \times 2.5^{\circ}$	30
#13	14–25 September 2009	Heelis	3.0	$2.5^{\circ} \times 2.5^{\circ}$	1
#14	14–25 September 2009	Weimer	3.0	$2.5^{\circ} \times 2.5^{\circ}$	30
#15	14–25 September 2009	Weimer	3.0	$2.5^{\circ} \times 2.5^{\circ}$	1
#16	14–25 September 2009	Heelis	3.0	$1.25^{\circ} \times 1.25^{\circ}$	10
#17	14–25 September 2009	Heelis	3.0	$1.25^{\circ} \times 1.25^{\circ}$	5
#18	14–25 September 2009	Weimer	3.0	$1.25^{\circ} \times 1.25^{\circ}$	10
#19	14–25 September 2009	Weimer	3.0	$1.25^{\circ} \times 1.25^{\circ}$	5

2.2. TIE-GCM

The TIE-GCM is a global model of the coupled ionosphere-thermosphere system (Richmond et al., 1992). At the lower boundary (~ 96 km altitude), atmospheric dynamics are driven by the Global Scale Wave Model (GSWM, Hagan & Forbes, 2002, 2003). The high-latitude magnetospheric coupling and the resulting polar plasma convection can be specified by various convection models. For this study, multiple TIE-GCM runs with varying settings have been performed and analyzed. Table 1 summarizes all investigated model runs. The vertical resolution is 0.25 scale heights of the atmospheric pressure in all model runs. The applied plasma convection models are introduced in Section 2.3.

2.3. Convection Models

There are multiple ways to parameterize the polar plasma convection. The four models applied in this study are:

- **Heelis** is an empirical convection model that applies the Kp index as key parameter (Heelis et al., 1982).
- **Weimer** is an empirical convection model that applies the solar wind speed and density as well as the B_y and B_z components of the interplanetary magnetic field (Weimer, 1995, 2005).
- The *Assimilative Mapping of Ionospheric Electrodynamics* **AMIE** maps the polar plasma potential from ground and satellite magnetometer and SuperDARN plasma drift measurements (Richmond & Kamide, 1988).
- The *Assimilative Mapping of Geospace Observations* **AMGeO** is an expansion of the AMIE procedure (Matsuo, 2020). The main difference compared to AMIE is the reformulation of the best linear unbiased estimation problem as a Bayesian estimation problem (Matsuo, 2020). The AMGeO forcing applied in this paper was generated without space-based magnetometers.

3. Results

3.1. Model Version, Grid Resolution, and Convection Parameterization

Due to the substantial variation in Joule heating rates with geomagnetic activity, we will investigate three activity levels—“low” ($Kp < 2$), “moderate” ($2 < Kp < 6$), and “high” ($Kp > 6$)—separately. A linear interpolation of the 3-hourly Kp index is performed, and the median model and EISCAT-derived Joule heating rates are calculated. We want to highlight that due to the different neutral atmosphere parameters in the model runs listed in Table 1, a separate “EISCAT profile” is calculated for each of the 19 model runs. Figure 1a shows the Joule heating profiles of the TIE-GCM 3.0 runs with 1.25° grid resolution (#2 Heelis; #5 Weimer; #8 AMIE; #11 AMGeO). The mean of the four EISCAT-derived profiles is shown as “EISCAT,” since the standard deviation of the four profiles is consistently below 10% in all regimes, which is sufficiently low for a qualitative comparison. For the TIE-GCM Joule heating profiles, the default scaling factor $f = 1.5$ has been applied. The values in the figure legend give the height-integrated Joule heating rates for each profile.

At low geomagnetic activity $Kp < 2$ (6.5% of all measurements), the Heelis-, Weimer-, and AMIE-driven profiles resemble the EISCAT-derived profile well. However, the Weimer- and AMIE-driven runs underestimate the Joule heating rate below 115 km altitude, and the Heelis-driven run struggles to reproduce the profile shape. The AMGeO-driven model run underestimates the Joule heating rate at all altitudes.

At moderate geomagnetic activity $2 < Kp < 6$ (76.1%), the model runs driven by AMIE and AMGeO reproduced the measurement-derived profile well. The Heelis- and Weimer-driven runs overestimate the peak Joule heating rate at about 120 km altitude.

At high geomagnetic activity $Kp > 6$ (17.4%), the AMIE- and AMGeO-driven runs also perform better than the model runs driven by empirical convection models. The Heelis-/Weimer-driven runs strongly over-/underestimate the Joule heating rates. AMIE-driven runs reproduce the profile generally well but tend to overestimate the peak Joule heating rate, whereas the AMGeO-driven run reproduces the shape of the profile well but underestimates the Joule heating rates at all altitudes.

Figure 1b shows the ratios of Joule heating rates in 1.25° and 2.5° model runs. The higher horizontal resolution results in increased Joule heating rates by 20% on average. The resolution impact ranges from -10% (Weimer; $Kp > 6$) to $+38\%$ (Heelis; $Kp < 2$). Figure 1c shows the ratios of Joule heating rates in TIE-GCM 3.0 and 2.0 runs, both with 2.5° grid resolution. There is no clear trend of whether the different versions result in generally increased/decreased Joule heating rates. It stands out, though, that the model runs driven with the assimilative AMIE technique show strong variations of Joule heating rates with the model version, ranging from $+10\%$ at $Kp < 2$ to -37% at $Kp > 6$. Note that all percentages are given for height-integrated Joule heating rates.

To quantitatively assess the agreement of model and measurement-derived Joule heating rates, we calculate ϵ_N from Equation 2 for each of the model runs #1–#11 from Table 1. Figure 2 shows ϵ_N (a) if the default $f = 1.5$ Joule heating scaling is applied and (b) if an adjusted scaling factor is applied. It can be seen in Figure 2a that despite the normalization, ϵ_N is larger for high geomagnetic activity. ϵ_N is lowest for moderate geomagnetic activity for which the $f = 1.5$ scaling has been determined in Codrescu et al. (1995).

For $f = 1.5$, AMIE-driven TIE-GCM runs show the best agreement of Joule heating rates with our EISCAT calculations. Notably, the 1.25° resolution run (#8) has the lowest ϵ_N for moderate and high geomagnetic activity, while the version 3.0/ 2.5° resolution run (#7) agrees better at $Kp < 2$. It can be seen in Figure 2a that, at low and high geomagnetic activity, the agreement of AMIE-driven runs with EISCAT is improved for model version 3.0. Averaged over all three Kp bins, the agreement with the EISCAT-derived Joule heating rates is 45% higher. When comparing empirical and data-assimilated geomagnetic forcing, we find that ϵ_N is decreased by 8%, 28%, and 54% for low, moderate, and high geomagnetic activity.

ϵ_N for the adjusted scaling factor Joule scaling rates in Figure 2b can be seen as a measure of how well the model reproduces the shape of the profile (see Section 3.2). It can be seen that AMGeO-driven TIE-GCM runs agree best with the EISCAT-derived profiles for $Kp < 2$ and $Kp > 6$. This suggests that AMIE-driven runs reproduce the overall magnitude of Joule heating best, while AMGeO-driven runs reproduce the shape of the profiles at low and high geomagnetic activity best.

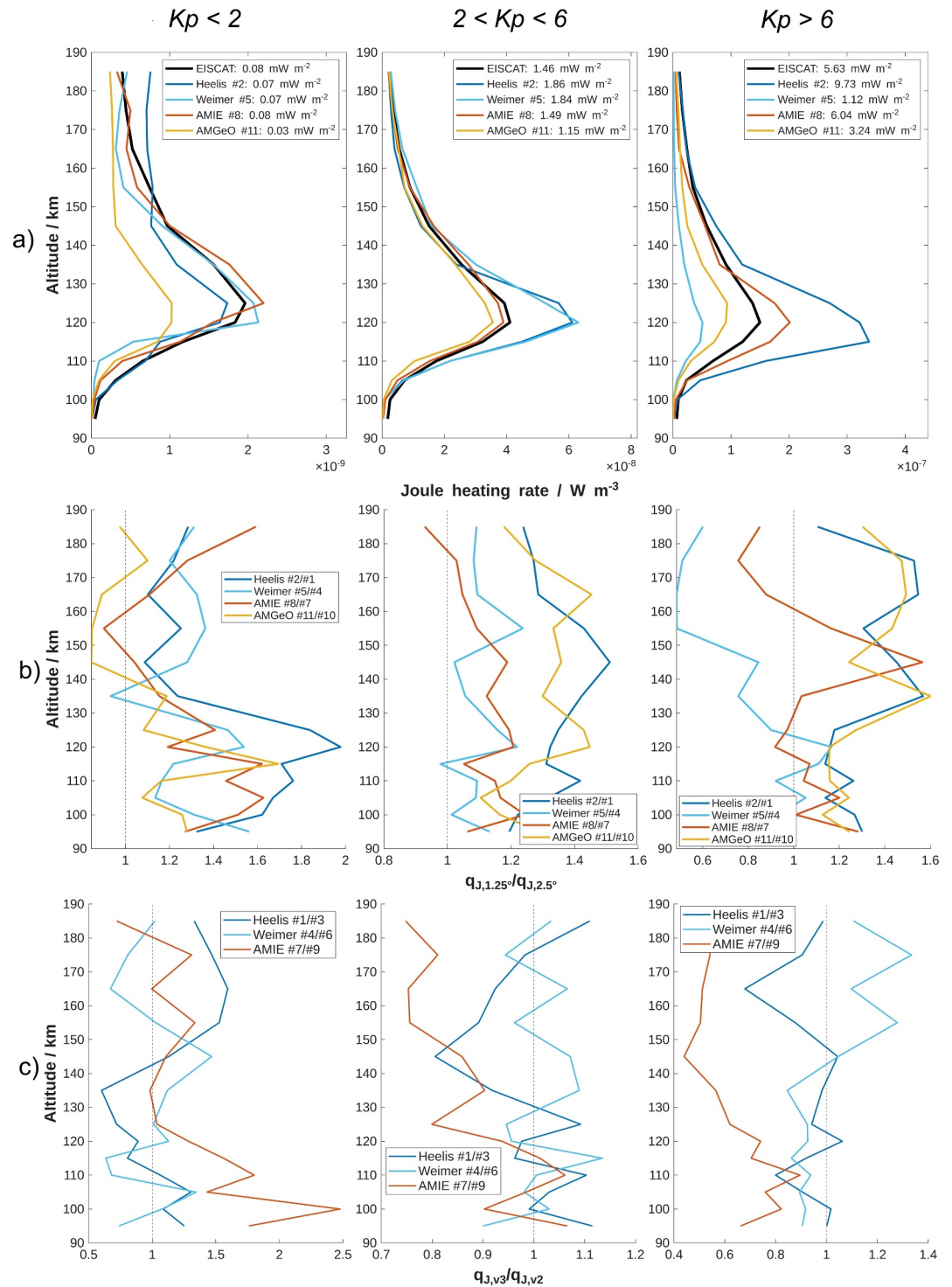


Figure 1. (a) Joule heating rate profiles for Thermosphere Ionosphere Electrodynamics General Circulation Model (TIE-GCM) 3.0 runs with 1.25° grid resolution. The profiles are binned by geomagnetic activity, and the median profile is shown for each bin. The EISCAT profile is calculated separately for each model run, and the mean EISCAT profile is shown. Ratio of Joule heating rates in (b) 1.25° and 2.5° grid resolution runs and (c) TIE-GCM 3.0 and 2.0 runs (both with 2.5° grid resolution).

From Equation 1, it can be seen that two EISCAT measurements, the electron density N_e and the ion velocity \vec{v}_i from which the electric field \vec{E} is calculated, affect the Joule heating rate. Since both these quantities are affected by the geomagnetic forcing at high latitudes, we need to distinguish their contributions to ϵ_N .

Figure 3 shows the ratios of (a) model-to-EISCAT electron density and (b) the $\vec{E} + \vec{u} \times \vec{B}$ -term (see Equation 1) calculated from the model and the EISCAT measurements. It is apparent in Figure 3a that all model runs underestimate the electron density below 100 km altitude and overestimate it above. At moderate and high geomagnetic activity, this overestimation is stronger for Heelis- and Weimer-driven runs. This explains the overestimation of Joule heating rates for these runs at moderate and for Heelis-driven runs at high geomagnetic activity. The fact that Weimer-driven runs underestimate the Joule heating rate at $Kp > 6$ is caused by the underestimation of the $\vec{E} + \vec{u} \times \vec{B}$ -term (Figure 3b, right panel). The $\vec{E} + \vec{u} \times \vec{B}$ -ratio is mainly determined by the electric fields, while the variability with altitude is due to changing neutral wind directions. Figure 3 demonstrates that the lower ϵ_N for AMIE- and AMGeO-driven runs is mainly due to a better agreement of model and EISCAT electron density. AMGeO-driven runs show the least altitudinal variation of both N_e and $\vec{E} + \vec{u} \times \vec{B}$ ratio. Therefore, adjusting the constant scaling factor can overcome most deviations of the model and measurement-derived profile. This explains why the AMGeO-driven runs show a lower ϵ_N for an adjusted scaling factor f .

3.2. Model Time Step and Profile Shape

It can be seen in Table 1 that the model time steps Δt for runs #1–#11 (September 2005) were varied from the default setting $\Delta t = 30$ s down to $\Delta t = 5$ s. This is necessary since the model can be numerically unstable under storm conditions for the default time step. To keep the modeling procedure efficient, the internal time steps were set to the default value whenever feasible and only decreased when necessary. However, this is only justified if the different internal model time steps do not affect the Joule heating rates.

We performed separate model runs for the EISCAT campaign from 14 to 25 September 2009, which was conducted under generally low geomagnetic activity $Kp \leq 3+$ and therefore allowed us to run a larger range of internal time steps without reaching numerical instability. In these runs, the model time steps were kept constant, and we tested two time steps for the grid resolution $1.25^\circ \times 1.25^\circ$ ($\Delta t_1 = 10$ s; $\Delta t_2 = 5$ s) and $2.5^\circ \times 2.5^\circ$ ($\Delta t_1 = 30$ s; $\Delta t_2 = 1$ s). Since no AMIE or AMGeO outputs were available for this time, this analysis is restricted to Heelis and Weimer convection forcing. The results are assumed to be representative.

Figure 4a shows a scatter plot of the model Joule heating rates for Δt_1 and Δt_2 . It can be seen that the Joule heating rates are highly correlated, suggesting that as long as the model does not evolve numerical instability, the Joule heating results converge for any reasonable model time step. The procedure applied for model runs #1–#11 of increasing and decreasing the internal model time steps to maximize the efficiency of the modeling process is therefore justified and does not affect the results.

Figure 4b shows a scatter plot of height-integrated Joule heating rates Q_J in all model runs #1–#11 over the corresponding EISCAT-derived Q_J . The correlation varies between the different runs, reaching as low as $R = 0.2$ for Weimer-driven run #6 and up to $R = 0.5$ for AMIE-driven run #7. This shows that even for the improved Joule heating representation in AMIE-driven runs, the correlation with measurements remains moderate.

Figure 4 compares the Joule heating rate profiles at $Kp > 6$ for (c) AMIE- and (d) AMGeO-driven model runs. It can be seen that for the default $f = 1.5$, the AMIE-driven model profile agrees better with the EISCAT-derived profile, even though the Joule heating rate at the peak altitude of 120 km is overestimated. If an adjusted scaling factor $f = 1.2$ is applied, the Joule heating rate is underestimated above 130 km altitude. The AMGeO-driven run underestimates the Joule heating rate at all altitudes. However, applying $f = 2.5$, the model and EISCAT-derived profiles agree better compared to the AMIE-driven run.

4. Discussion and Conclusions

Since the presented study is limited to two EISCAT campaigns, conclusions have to be drawn carefully. Our main conclusions are:

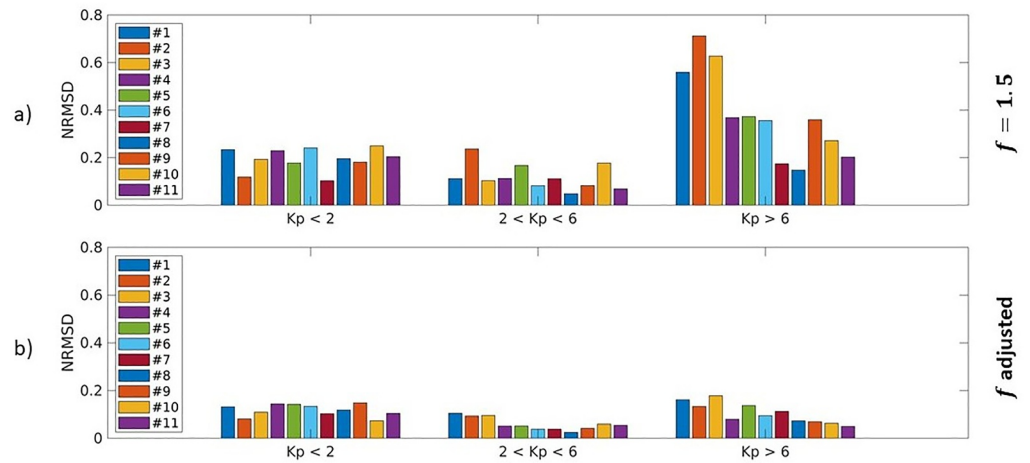


Figure 2. NRMSD of the modeled and EISCAT-derived Joule heating rate profiles for (a) the default scaling factor $f = 1.5$ and (b) separately adjusted scaling factors for each model run.

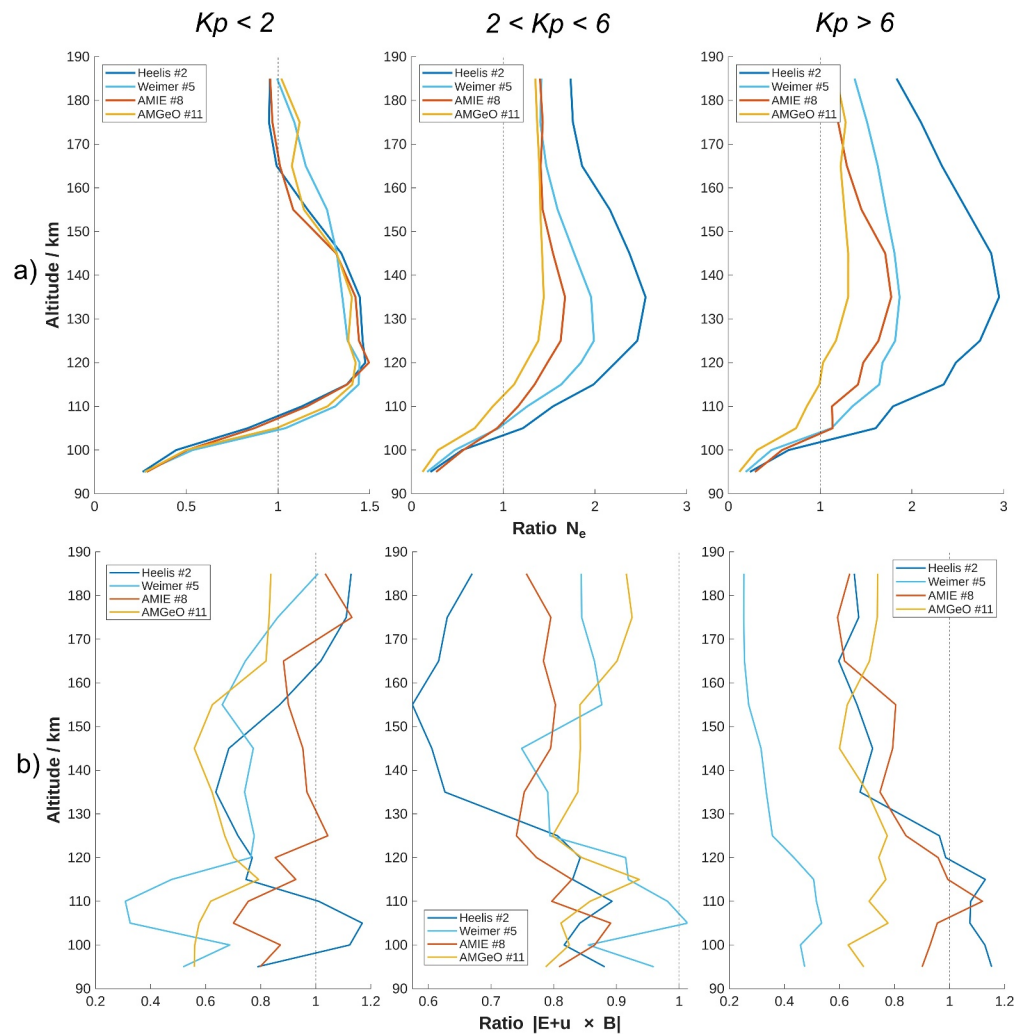


Figure 3. Model-to-EISCAT ratios of (a) electron density and (b) the dynamo electric field $\vec{E} + \vec{u} \times \vec{B}$ for 1.25° resolution runs.

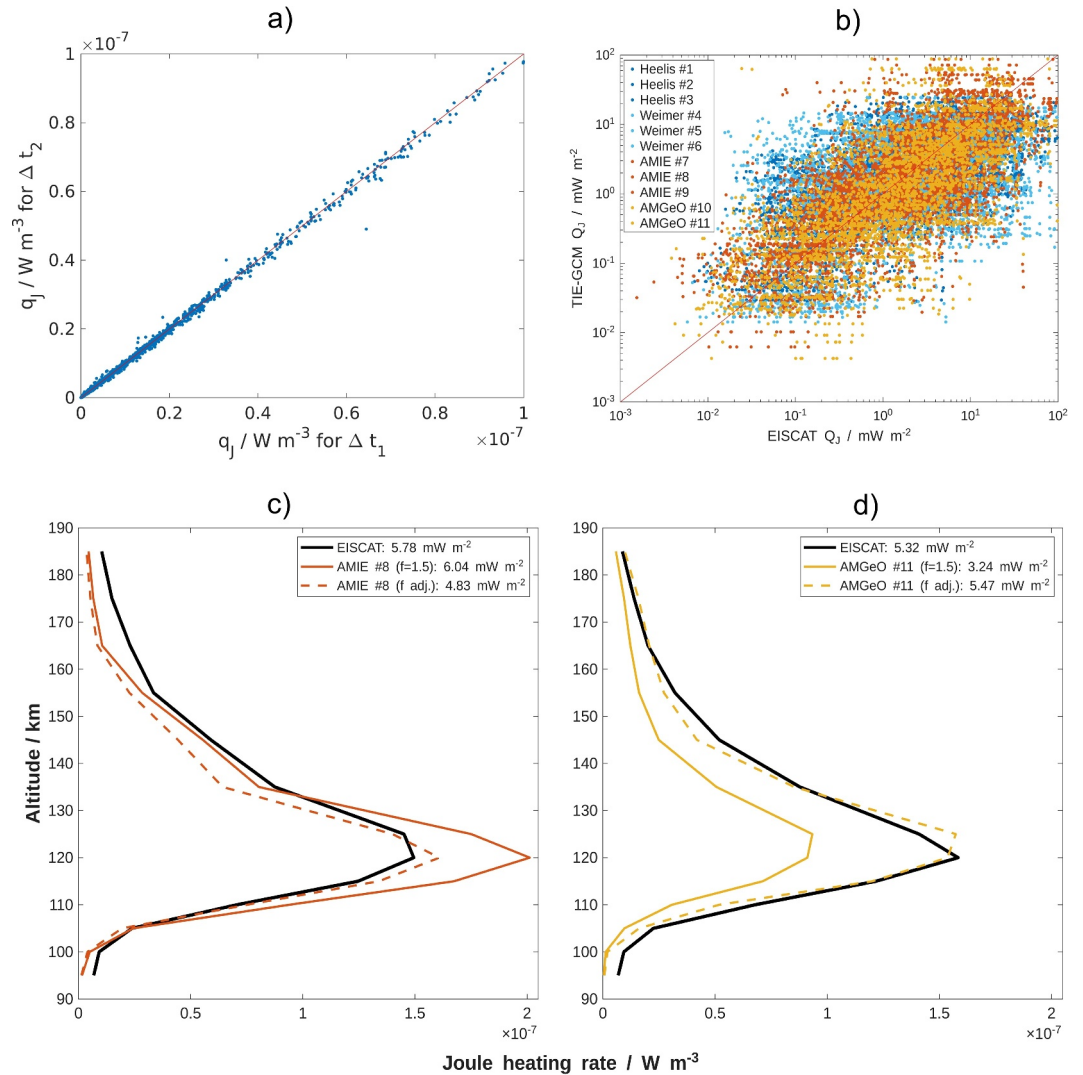


Figure 4. (a) Scatter plot of Joule heating rates for model runs with different internal time steps. (b) Scatter plot of height-integrated Joule heating rates calculated from EISCAT measurements and Thermosphere Ionosphere Electrodynamics General Circulation Model runs #1–#11. The Joule heating rate profiles for $K_p > 6$ for (c) AMIE- and (d) AMGeO-driven runs with the default $f = 1.5$ and adjusted scaling factors.

1. The high-latitude Joule heating in TIE-GCM agrees better with EISCAT measurements if the data-assimilated convection models AMIE and AMGeO are applied (compared to the empirical models Heelis and Weimer). For high geomagnetic activity, ϵ_N is decreased by more than 50%.
2. AMGeO-driven runs reproduce the shape of the vertical Joule heating rate profile notably well.
3. The increased grid resolution (from 2.5° to 1.25°) results in generally higher height-integrated Joule heating rates by 20% on average.
4. The new TIE-GCM version 3.0 improves the agreement of Joule heating rates in AMIE-driven runs and EISCAT measurements by about 45%. However, there is no general trend when comparing all convection models.
5. The internal model time step does not affect the Joule heating rates and hence can be adjusted to make the modeling process more efficient.

The better agreement of model and measurement parameters for data-assimilated geomagnetic forcing agrees well with previous studies investigating AMIE- (e.g., Davidson et al., 2025; Lu et al., 1998, 2001) and AMGeO-driven (e.g., Hsu & Pedatella, 2023; Hsu et al., 2021) TIE-GCM runs. However, these studies have mostly been

restricted to single events, mainly under storm conditions. A systematic evaluation of modeled Joule heating rates for multiple convection models and the entire range of geomagnetic activity levels was so far missing. The impact of model resolution on the Joule heating rates is similar to the effect of short-term variability discussed in Codrescu et al. (1995). The increased Joule heating rates for higher grid resolution might be caused by the smaller-scale variability of electron density (and therefore Pedersen conductivity) and electric fields. The general underestimation of Joule heating rates reported in previous studies (Baloukidis et al., 2023; Codrescu et al., 1995; Günzkofer et al., 2024) is partially mitigated by the improved spatial resolution in TIE-GCM 3.0. The most likely cause for the differences between model versions is the updated thermal electron heating rate in TIE-GCM 3.0 (Wu et al., 2025). When the scaling factor was adjusted, AMGeO-driven runs exhibited a better agreement than AMIE-driven runs for low and high geomagnetic activity. This indicates that AMGeO-driven runs reproduce the shape of the Joule heating rate profile better. We could identify that the overestimation of Joule heating rates by Heelis-driven runs at $Kp > 6$ is caused by the electron density while the underestimation by Weimer-driven runs is caused by the $\vec{E} + \vec{u} \times \vec{B}$ -term. Therefore, when investigating storm conditions, assimilative convection models should be applied.

Future research on high-latitude Joule heating should aim for an extended investigation of TIE-GCM runs driven with data-assimilated convection models. While we limited the analysis to two EISCAT campaigns in this initial study, extending the investigated measurements is possible by either limiting the number of model runs (and therefore settings) or dedicating a larger amount of resources. Another important point is the extension of the measurement capabilities. The Poker Flat Incoherent Scatter Radar (PFISR) is located at about the same geomagnetic latitude as the EISCAT Tromsø radar and on the opposite side of the polar region. Should the adjusted scaling for EISCAT and PFISR be comparable, adjusting the global scaling factor as suggested by Günzkofer et al. (2024) might be applicable for single geomagnetic latitudes. However, due to the small-scale variability of electric fields as demonstrated by Codrescu et al. (2000), global scaling of Joule heating rates might be generally limited in accuracy. The phased-array radar PFISR would allow for some horizontal coverage and thereby investigate this short-scale variability. Similar investigations will be possible for the European sector with the upcoming EISCAT_3D system (McCrea et al., 2015).

Acknowledgments

EISCAT is an international association supported by research organizations in China (CRIRP), Finland (SA), Japan (NIPR and ISEE), Norway (NFR), Sweden (VR), and the United Kingdom (UKRI). The TIE-GCM and related Thermosphere-Ionosphere models have been developed by the “Atmosphere Ionosphere Magnetosphere” (AIM) Section of the High Altitude Observatory (HAO) at NCAR (see <http://www.hao.ucar.edu/modeling/tgcm>). The National Center for Atmospheric Research is a major facility sponsored by the National Science Foundation under Cooperative Agreement 1852977. GS is a member of the Oeschger Center for Climate Change Research (OCCR). AMGeO is supported by the NSF EarthCube grants ICER 1928403 to the University of Colorado Boulder, ICER 1928327 to the Virginia Tech, and ICER 1928358 to the Johns Hopkins University Applied Physics Laboratory. We are grateful to the community data providers (NASA SPDF, SuperMAG, and SuperDARN) for providing data for the community, such that they can be used in AMGeO. HL acknowledges support from JSPS KAKEN Grants JP25K01058 and JP22K21345. GL was supported by NASA Grants 80NSSC20K1784 and 80NSSC21K1673. The internal pre-review at DLR-SO by Gloria Tan Jun Rios is gratefully acknowledged. Open Access funding enabled and organized by Projekt DEAL.

Inclusion in Global Research Statement

This work was conducted in large parts during a 2-month stay of Florian Günzkofer with the High Altitude Observatory (HAO) of the National Center for Atmospheric Research (NCAR). The scientific visitor opportunity was supported by both HAO/NCAR and the German Aerospace Center (DLR).

Data Availability Statement

The data shown in this manuscript and the software required to reproduce the figures can be obtained from Günzkofer et al. (2025). All data and software are available under the Creative Commons Attribution 4.0 International license. In case of further questions about the data or the analysis software, please contact the corresponding author.

References

- Alken, P., Thébault, E., Beggan, C. D., Amit, H., Aubert, J., Baerenzung, J., et al. (2021). International geomagnetic reference field: The thirteenth generation. *Earth Planets and Space*, 73(1), 49. <https://doi.org/10.1186/s40623-020-01288-x>
- Baloukidis, D., Sarris, T., Tourgaidis, S., Pinaris, P., Aikio, A., Virtanen, I., et al. (2023). A comparative assessment of the distribution of joule heating in altitude as estimated in TIE-GCM and EISCAT over one solar cycle. *Journal of Geophysical Research (Space Physics)*, 128(12), e2023JA031526. <https://doi.org/10.1029/2023JA031526>
- Codrescu, M. V., Fuller-Rowell, T. J., & Foster, J. C. (1995). On the importance of E-field variability for Joule heating in the high-latitude thermosphere. *Geophysical Research Letters*, 22(17), 2393–2396. <https://doi.org/10.1029/95GL01909>
- Codrescu, M. V., Fuller-Rowell, T. J., Foster, J. C., Holt, J. M., & Cariglia, S. J. (2000). Electric field variability associated with the Millstone Hill electric field model. *Journal of Geophysical Research: Space Physics*, 105(A3), 5265–5274. <https://doi.org/10.1029/1999JA900463>
- Davidson, K., Lu, G., & Conde, M. (2025). Effects of high-latitude input on neutral wind structure and forcing during the 17 March 2013 storm. *Journal of Geophysical Research (Space Physics)*, 130(3), 2024JA033366. <https://doi.org/10.1029/2024JA033366>
- Emery, B. A., Lathuillere, C., Richards, P. G., Roble, R. G., Buonsanto, M. J., Knipp, D. J., et al. (1999). Time dependent thermospheric neutral response to the 2–11 November 1993 storm period. *Journal of Atmospheric and Solar-Terrestrial Physics*, 61(3–4), 329–350. [https://doi.org/10.1016/S1364-6826\(98\)00137-0](https://doi.org/10.1016/S1364-6826(98)00137-0)
- Folkestad, K., Hagfors, T., & Westerlund, S. (1983). EISCAT: An updated description of technical characteristics and operational capabilities. *Radio Science*, 18(6), 867–879. <https://doi.org/10.1029/RS018i006p00867>

- Günzkofer, F., Liu, H., Liu, H., Stober, G., Lu, G., Wu, H., et al. (2025). High-latitude Joule heating in TIE-GCM 3.0: Impact of model version, convection forcing, and grid resolution evaluated with EISCAT measurements [Dataset]. *Zenodo*. <https://doi.org/10.5281/zenodo.15637976>
- Günzkofer, F., Liu, H., Stober, G., Pokhotelov, D., & Borries, C. (2024). Evaluation of the empirical scaling factor of Joule heating rates in TIE-GCM with EISCAT measurements. *Earth and Space Science*, 11(4), e2023EA003447. <https://doi.org/10.1029/2023EA003447>
- Hagan, M. E., & Forbes, J. M. (2002). Migrating and nonmigrating diurnal tides in the middle and upper atmosphere excited by tropospheric latent heat release. *Journal of Geophysical Research (Atmospheres)*, 107(D24), 4754. <https://doi.org/10.1029/2001JD001236>
- Hagan, M. E., & Forbes, J. M. (2003). Migrating and nonmigrating semidiurnal tides in the upper atmosphere excited by tropospheric latent heat release. *Journal of Geophysical Research (Space Physics)*, 108(A2), 1062. <https://doi.org/10.1029/2002JA009466>
- Heelis, R. A., Lowell, J. K., & Spiro, R. W. (1982). A model of the high-latitude ionospheric convection pattern. *Journal of Geophysical Research*, 87(A8), 6339–6345. <https://doi.org/10.1029/JA087iA08p06339>
- Hsu, C. T., Matsuo, T., Maute, A., Stoneback, R., & Lien, C. P. (2021). Data driven ensemble modeling of equatorial ionospheric electrodynamics: A case study during a minor storm period under solar minimum conditions. *Journal of Geophysical Research*, 126(2), e28539. <https://doi.org/10.1029/2020JA028539>
- Hsu, C. T., & Pedatella, N. M. (2023). Effects of forcing uncertainties on the thermospheric and ionospheric states during geomagnetic storm and quiet periods. *Space Weather*, 21(4), e2022SW003216. <https://doi.org/10.1029/2022SW003216>
- Kauristie, K., Marghitu, O., van de Kamp, M., Hoppe, T., Honkonen, I., Blagau, A., et al. (2024). Joule Heating rate at high-latitudes by Swarm and ground-based observations compared to MHD simulations. *Journal of Atmospheric and Solar-Terrestrial Physics*, 260, 106254. <https://doi.org/10.1016/j.jastp.2024.106254>
- Kavanagh, A. J., Ogawa, Y., & Woodfield, E. E. (2022). Two techniques for determining F-Region ion velocities at meso-scales: Differences and impacts on Joule heating. *Journal of Geophysical Research*, 127(6), e30062. <https://doi.org/10.1029/2021JA030062>
- Lu, G., Pi, X., Richmond, A. D., & Roble, R. G. (1998). Variations of total electron content during geomagnetic disturbances: A model/observation comparison. *Geophysical Research Letters*, 25(3), 253–256. <https://doi.org/10.1029/97GL03778>
- Lu, G., Richmond, A. D., Roble, R. G., & Emery, B. A. (2001). Coexistence of ionospheric positive and negative storm phases under northern winter conditions. *A case study*, 106(A11), 24493–24504. <https://doi.org/10.1029/2001JA000003>
- Matsuo, T. (2020). Recent progress on inverse and data assimilation procedure for high-latitude ionospheric electrodynamics. In M. W. Dunlop & H. Lühr (Eds.), *Ionospheric multi-spacecraft analysis tools: Approaches for deriving ionospheric parameters* (Vol. 17, pp. 219–232). https://doi.org/10.1007/978-3-030-26732-2_10
- McCrea, I., Aikio, A., Alfonsi, L., Belova, E., Buchert, S., Clilverd, M., et al. (2015). The science case for the EISCAT_3D radar. *Progress in Earth and Planetary Science*, 2(1), 21. <https://doi.org/10.1186/s40645-015-0051-8>
- Nozawa, S., Ogawa, Y., Oyama, S., Fujiwara, H., Tsuda, T., Brekke, A., et al. (2010). Tidal waves in the polar lower thermosphere observed using the EISCAT long run data set obtained in September 2005. *Journal of Geophysical Research*, 115(A8), A08312. <https://doi.org/10.1029/2009JA015237>
- Nygrén, T., Aikio, A. T., Kuula, R., & Voiculescu, M. (2011). Electric fields and neutral winds from monostatic incoherent scatter measurements by means of stochastic inversion. *Journal of Geophysical Research (Space Physics)*, 116(A5), A05305. <https://doi.org/10.1029/2010JA016347>
- Palmroth, M., Janhunen, P., Pulkkinen, T. I., Aksnes, A., Lu, G., Østgaard, N., et al. (2005). Assessment of ionospheric Joule heating by GUMICS-4 MHD simulation, AMIE, and satellite-based statistics: Towards a synthesis. *Annales Geophysicae*, 23(6), 2051–2068. <https://doi.org/10.5194/angeo-23-2051-2005>
- Rich, F. J., Gussenhoven, M. S., Hardy, D. A., & Holeman, E. (1991). Average height-integrated Joule heating rates and magnetic deflection vectors due to field-aligned currents during sunspot minimum. *Journal of Atmospheric and Terrestrial Physics*, 53(3–4), 293–308. [https://doi.org/10.1016/0021-9169\(91\)90113-L](https://doi.org/10.1016/0021-9169(91)90113-L)
- Richmond, A. D., & Kamide, Y. (1988). Mapping electrodynamic features of the high-latitude ionosphere from localized observations. *Technique*, 93(A6), 5741–5759. <https://doi.org/10.1029/JA093iA06p05741>
- Richmond, A. D., Ridley, E. C., & Roble, R. G. (1992). A thermosphere/ionosphere general circulation model with coupled electrodynamics. *Geophysical Research Letters*, 19(6), 601–604. <https://doi.org/10.1029/92GL00401>
- Thayer, J. P. (2000). High-latitude currents and their energy exchange with the ionosphere-thermosphere system. *Journal of Geophysical Research*, 105(A10), 23015–23024. <https://doi.org/10.1029/1999JA000409>
- Weimer, D. R. (1995). Models of high-latitude electric potentials derived with a least error fit of spherical harmonic coefficients. *Journal of Geophysical Research*, 100(A10), 19595–19608. <https://doi.org/10.1029/95JA01755>
- Weimer, D. R. (2005). Improved ionospheric electrodynamic models and application to calculating Joule heating rates. *Journal of Geophysical Research (Space Physics)*, 110(A5), A05306. <https://doi.org/10.1029/2004JA010884>
- Wu, H., Wang, W., Pham, K. H., Lin, D., Rao, N., Wiltberger, M., et al. (2025). *The NCAR-TIEGCM Version 3.0*. ESS Open Archive. <https://doi.org/10.22541/essoar.174835358.89263150/v1>